

oscillatory heat flux, mimicking a step-like function intercalating periods of constant heating with periods of constant cooling, is imposed uniformly at the top surface. For a Newtonian fluid with constant properties (except density in the buoyancy term), the nondimensional time-dependent conservation equations of mass, momentum, and energy are, respectively,

$$\frac{\partial U}{\partial X} + \frac{\partial V}{\partial Y} = 0 \tag{1}$$

$$\frac{DU}{D\tau} = -\frac{\partial P}{\partial X} + \left(\frac{Pr}{Ra}\right)^{1/2} \nabla^2 U \tag{2}$$

$$\frac{DV}{D\tau} = -\frac{\partial P}{\partial Y} + \left(\frac{Pr}{Ra}\right)^{1/2} \nabla^2 V + \theta \tag{3}$$

$$\frac{D\theta}{D\tau} = \frac{1}{(RaPr)^{1/2}} \nabla^2 \theta \tag{4}$$

Nondimensional variables and parameters in Equations 1 to 4 and Figure 1 are

$$(X, Y) = \frac{(x, y)}{H}, (U, V) = \frac{(u, v)}{\frac{\alpha}{H}(RaPr)^{1/2}}, \tau = \frac{\alpha(RaPr)^{1/2}}{H^2} t, \tag{5}$$

$$\theta = \frac{T - T_0}{q_m'' \left(\frac{H}{k}\right)}, Pr = \frac{\nu}{\alpha}, P = \frac{H^2 (p + \rho g y)}{\rho \alpha^2 RaPr}, Ra = \frac{g \beta q_m'' H^4}{\alpha \nu k},$$

$$Q'' = \frac{q''}{q_m''}, (\Omega_h, \Omega_c) = (t_h, t_c) \frac{\alpha}{H^2} (RaPr)^{1/2}$$

with dimensional quantities defined in the nomenclature. It is worth noting at this point that q_m'' is a positive dummy constant used only for nondimensionalizing q'' ; consequently, the usual heat-flux-based Rayleigh number, Ra_q , is in fact equal to $Q'' Ra$ (following the thermodynamic convention $Q'' < 0$ when cooling the reservoir).

In writing Equations 1 to 4, the maximum absolute value of the temperature difference ($T_1 - T_0$) is assumed to be smaller

than $0.4 T_0$, in which case the invoked Oberbeck–Boussinesq approximation is reasonably accurate (Frohlich et al. 1992).

Physical parameters

Four independent parameters govern the heating process, namely, amplitudes Q''_h and Q''_c , and periods Ω_h and Ω_c (Figure 1). This investigation is restricted to the case $Q''_h = Q''_c = |Q''|$ and $\Omega_h = \Omega_c = \Omega$. The heat flux frequency is then $f = 1/(2\Omega)$.

Heat transfer parameters of interest are the top and bottom surface averaged temperatures, respectively,

$$\theta_t = \int_0^1 \theta|_{Y=1} dX \quad \text{and} \quad \theta_b = \int_0^1 \theta|_{Y=0} dX \tag{6}$$

and the midheight averaged Nusselt number,

$$Nu_v = \frac{-q'_v}{q_m'' L} = \frac{H}{L} \int_0^1 -\left[(RaPr)^{1/2} V \theta - \frac{\partial \theta}{\partial Y} \right]_{Y=1/2} dX \tag{7}$$

The top surface averaged Nusselt number is

$$Nu_t = \frac{q_m''}{T_1 - T_0} \frac{H}{k} = \frac{1}{\theta_t} \tag{8}$$

Another parameter, important for the detection of fluid motion (convection) within the reservoir, is the volume-averaged root-mean-square velocity

$$\omega = \frac{1}{\mathfrak{V}} \sqrt{\sum_{i,j} \{ \varphi_{i,j} [U(i,j)^2 + V(i,j)^2] \}} \tag{9}$$

where $\varphi_{i,j}$, $U(i,j)$, and $V(i,j)$ are, respectively, volume and velocities at each node (i,j) within the domain, and \mathfrak{V} is the total volume of the reservoir.

Numerical method

The finite-volume method, previously applied and validated for similar problems (Lage and Bejan 1992; Antohe and Lage 1993), is used here with the SIMPLE algorithm (Patankar 1980)

Notation		Greek symbols	
d	Cooling-front thickness, m	α	Thermal diffusivity, m^2/s
g	Gravity acceleration, m^2/s	β	Isobaric thermal expansion coefficient, K^{-1}
H	Height of fluid reservoir, m	δ	Nondimensional cooling-front thickness
k	Thermal conductivity, W/mK	φ, \mathfrak{V}	Nondimensional volumes, Equation 9
L	Width of fluid reservoir, m	ν	Kinematic viscosity, m^2/s
Nu	Nusselt number, Equations 7 and 8	θ	Nondimensional temperature, Equation 5
P	Pressure, Pa	ρ	Density, kg/m^3
Pr	Prandtl number, Equation 5	τ	Nondimensional time, Equation 5
q''	Heat flux, W/m^2	ω	Root mean square velocity, Equation 9
Q''	Nondimensional heat flux, Equation 5	Ω	Nondimensional time period, Equation 5
Ra	Rayleigh number, Equation 5		
t	Time, s		
T	Temperature, K		
u, v	Horizontal and vertical velocities, m/s		
U, V	Nondimensional horizontal and vertical velocities, Equation 5		
x, y	Horizontal and vertical coordinates, m		
X, Y	Nondimensional horizontal and vertical coordinates, Equation 5		
		Subscripts	
		b	Bottom
		c	Critical
		e	Cooling
		h	Heating
		t	Top

and the QUICK scheme (Leonard 1979). The discretized equations are solved using an implicit alternating-direction Gauss-Seidel iterative method and the efficient Tri-Diagonal-Matrix Thomas algorithm. The time-integration scheme is a second-order Crank-Nicholson predictor-corrector method, implemented as suggested by Patterson and Armfield (1990). The present numerical code is verified also against the results reported by Armfield and Patterson (1991).

Extensive grid accuracy tests are performed, following the same basic concepts described in detail by Manole and Lage (1992). Several different grid distributions are implemented, depending on the case. Considering $Ra_q = 8 \times 10^8$ and $Pr = 7$, for instance, optimum results are obtained with 120×120 grid lines, nonuniform distribution in the vertical direction, and time step equal to 10^{-4} . A coarser grid with 50×50 nodes and time step equal to 10^{-2} is used for $Ra_q = 10^3$ and the same Prandtl number.

All results reported here are at least 4% accurate considering a 20% increase in the total number of grid lines and a one-order-of-magnitude decrease in the time step. Attempts to resolve flow and temperature fields within this accuracy for higher Rayleigh number, e.g., $Ra_q = 10^{10}$, indicate the need for at least 200 nodes, pushing the CPU time to unrealistic values. The implementation of a turbulence model might be necessary in order to reduce the computation time.

Theoretical analysis

In this section, an approximate condition for the initiation of convection is derived considering a *continuous cooling* (from the top) process. Notice that although continuously heating the enclosure from the top leads to a stable configuration, it is shown later on that convection can be induced by heating/cooling the enclosure even when the cycling process starts with heating.

During cooling, a cold fluid front develops downwards with the top surface temperature decreasing continuously with time. During the initial cooling stage, when the heat transfer mode is that of conduction, Equation 4 simplifies to

$$\frac{\partial \theta}{\partial \tau} = \frac{1}{(RaPr)^{1/2}} \frac{\partial^2 \theta}{\partial Y^2} \tag{10}$$

An analytical solution of Equation 10, with isothermal initial condition, constant heat flux (Q'') at $Y = 1$, and zero heat flux ($\partial \theta / \partial Y = 0$) at $Y = 0$, was pioneered by Smith (1941). In terms of the nondimensional variables listed in Equation 5, the solution is

$$\frac{\theta}{Q''} = \frac{\tau}{(RaPr)^{1/2}} + \frac{3Y^2 - 1}{6} - \frac{2}{\pi^2} \times \sum_{n=1}^{\infty} \left\{ (-1)^n \frac{\cos(n\pi Y)}{n^2} \exp \left[\frac{-(n\pi)^2 \tau}{(RaPr)^{1/2}} \right] \right\} \tag{11}$$

By evaluating Equation 11 numerically, it is verified that when $\tau \geq \tau_b$, with

$$\tau_b = 0.2(RaPr)^{1/2} \tag{12}$$

the temperature ratio $\theta_{Y=0} / \theta_{Y=1}$ is larger than 0.1, a strong evidence that the cooling front has reached the bottom of the enclosure. Another important characteristic, as pointed out by Brooks (1958), is that when $\tau \geq \tau_{max}$, where

$$\tau_{max} = 0.4(RaPr)^{1/2} \tag{13}$$

the summation term of Equation 11 becomes negligible, and the temperature difference throughout the cooling layer,

($\theta_{Y=1} - \theta_{Y=0}$), approaches its maximum value of $0.5 Q''$ within less than 1%. The information contained in Equations 12 and 13 is essential for studying the critical condition for onset of convection within the reservoir, as discussed next.

Figure 2 presents the space and time evolution of the cooling front, Equation 11, considering $Ra = 10^4$ and $Pr = 7$, for several (Q'', τ) pairs. Clearly, the time rate of top temperature change is proportional to Q'' (compare the pairs: $(-0.1, 5)$, $(-1, 5)$, and $(-10, 5)$). The three lower curves, for $Q'' = -10$, indicate how the cooling front develops in time towards the bottom of the reservoir ($Y = 0$), as indicated by the arrows (a) and (b). For a fluid with density dependent only upon temperature and positive coefficient of thermal expansion, the fluid layer near the top becomes increasingly heavier with time, which might lead eventually to an unstable situation. During the time evolution of the cooling front, three possibilities exist:

- (1) slow top surface temperature decrease and shallow reservoir: an unstable temperature gradient is not achieved, so the fluid cools down indefinitely by conduction;
- (2) fast top surface temperature decrease and deep reservoir: an unstable gradient is achieved, so convection sets in; moving fluid is initially bounded by a *rigid* surface from the top and by a *free* surface from the bottom; and
- (3) fast top surface temperature decrease and shallow reservoir: unstable gradient is achieved, so convection sets in; moving fluid is bounded by *rigid* surfaces.

It is postulated here that the instability of the cooling layer is determined by a *local* and *instantaneous* Rayleigh number, defined as

$$Ra_\delta = \frac{g\beta(T_\delta - T_i)d^3}{\alpha\nu} \tag{14}$$

with d being the dimensional thickness of the cooling-front layer measured from the top, and $(T_\delta - T_i)$ the temperature difference across the layer. Note that d varies with time until the bottom of the reservoir is reached by the cooling front (when $d = H$) at $\tau = \tau_b$ (Equation 12). The across-the-layer temperature difference, $(T_\delta - T_i)$, then approaches its asymptotic maximum value at $\tau = \tau_{max}$ (Equation 13). The hypothesis behind Equation 14 was mentioned, in passing, by Lick (1965).

The Rayleigh number of Equation 14 is related to the Rayleigh number Ra define in Equation 5,

$$Ra_\delta = (\theta_\delta - \theta_i)\delta^3 Ra \tag{15}$$

where δ and $(\theta_\delta - \theta_i)$ are, respectively, the nondimensional cooling-front layer thickness ($\delta = d/H$) and the nondimensional temperature difference across the layer.

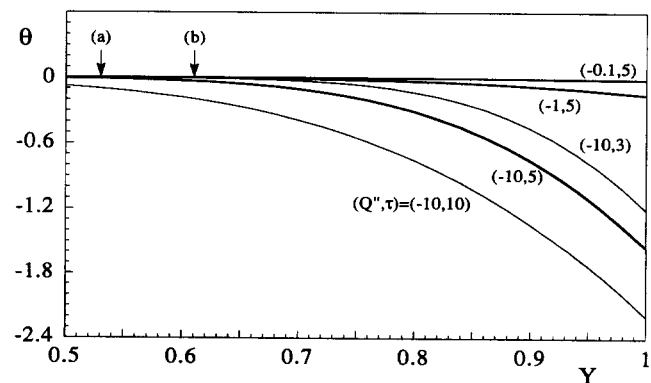


Figure 2 Pure conduction temperature profiles

Expressions for δ and $(\theta_\delta - \theta_1)$ are obtained by writing Equation 10 and the heat flux through the top surface in a scaling form, respectively,

$$\frac{(\theta_\delta - \theta_1)}{\tau} \sim \frac{1}{(\text{RaPr})^{1/2}} \frac{(\theta_\delta - \theta_1)}{\delta^2} \quad (16)$$

and

$$-Q'' = -\left. \frac{\partial \theta}{\partial Y} \right|_{Y=1} \sim \frac{\theta_\delta - \theta_1}{\delta} \quad (17)$$

Solving Equation 17 for δ and substituting the result into Equation 15 yields

$$\text{Ra}_\delta \sim \frac{(\theta_\delta - \theta_1)^4}{Q''^3} \text{Ra} \quad (18)$$

From Equations 16 and 17, the scale for $(\theta_\delta - \theta_1)$ is obtained as

$$\theta_1 - \theta_\delta \sim Q''(\text{RaPr})^{-1/4} \tau^{1/2} \quad (19)$$

Eliminating $(\theta_\delta - \theta_1)$ by combining Equations 18 and 19,

$$\text{Ra}_\delta \text{Pr} \sim Q'' \tau^2 \quad (20)$$

Equation 20 correlates total heat flux, Q'' , and total cooling time, τ , with the Boussinesq number equivalent, $\text{Ra}_\delta \text{Pr}$.

Notice that the time scale for the cooling front to reach the bottom of the enclosure can be obtained from Equation 16 by imposing $\delta = 1$. The result, $\tau_b \sim (\text{RaPr})^{1/2}$, differs only by a factor of 0.2 from the theoretical result predicted by Equation 12. Also, the maximum Ra_δ achievable within the enclosure during the cooling process can be obtained by comparing the time scale from Equation 20 with τ_{max} of Equation 13,

$$\text{Ra}_{\delta \text{max}} \sim 0.16 Q'' \text{Ra} \quad (21)$$

It is worth noting that the *actual* heat-flux-based Rayleigh number, Ra_q , is larger than the maximum-temperature-based Rayleigh number, $\text{Ra}_{\delta \text{max}}$.

The study of time-dependent density gradient instability differs from the studies of Rayleigh-Bénard instability (Chandrasekhar 1961), where a linear density profile is imposed. Nevertheless, a parallel is built in here between the two phenomena to obtain an approximated condition for the onset of convection. The strategy is very simple: for a certain fluid (Pr), using known values of critical Rayleigh number from the Rayleigh-Bénard studies in Equation 20, the minimum time for onset of convection is obtained for any given heat-flux amplitude, Q'' .

For a horizontal two-dimensional (2-D) thin-fluid-layer system (one that can have the vertical sidewall effect neglected, $L/H \rightarrow \infty$), Pellew and Southwell (1940) obtained, for a rigid-free configuration, a critical-temperature-based Rayleigh number equal to 1100.65. This is the case when the convective fluid has rigid-free horizontal bounds or, in other words, the critical cooling time for onset of convection, τ_c , is smaller than τ_b (Equation 12). The effect of vertical walls is expected to be minor in this case, especially when δ is relatively small when compared with the height of the enclosure, $Y = 1$. By setting $\text{Ra}_\delta \sim 1100.65$ in Equation 20, an estimate for the critical time, τ_c , for onset of convection is obtained,

$$\tau_c \sim 33 \left(\frac{\text{Pr}}{-Q''} \right)^{1/2} \quad (22)$$

provided that the thermal cooling layer does not reach the bottom surface, $\tau_b > \tau_c$. The minimum period, Ω , for the cooling process to induce convection, written in terms of critical (maximum) frequency, f_c , follows from Equation 22:

$$f_c \sim 0.015 \left(\frac{-Q''}{\text{Pr}} \right)^{1/2} \quad (23)$$

The analysis is now extended for $\tau \geq \tau_b$, in which case the convective fluid is bounded by rigid horizontal surfaces. In this situation, with $\delta = 1$, the vertical walls are expected to influence the onset of convection. Catton (1972) investigated the viscous effect, known to retard the onset of convection, of insulating vertical walls for a rigid-rigid horizontal configuration. Table 1 of his paper presents the critical Rayleigh number for several different aspect ratios. The values shown in the last line are good approximations for the critical Rayleigh number in a 2-D square configuration, namely, $\text{Ra}_{\delta=1} = 2453$. It follows from Equation 20 that

$$\tau_c \sim 50 \left(\frac{\text{Pr}}{-Q''} \right)^{1/2} \quad (24)$$

and, by consequence, that

$$f_c \sim 0.010 \left(\frac{-Q''}{\text{Pr}} \right)^{1/2} \quad (25)$$

provided $\tau_b \leq \tau_c$.

Equations 22 and 24 estimate the critical time for the onset of convection pending a comparison between the total cooling time and the bottom surface temperature time limit. In this regard, Foster (1965) had developed a theoretical linear stability analysis for a horizontally bounded infinite fluid layer. He considered two distinct cases concerning the top surface temperature: a step decrease and a linear decrease. He concluded, among other things, that for high Rayleigh numbers the critical time for the onset of convection is independent of the depth of the fluid layer. His conclusion, for the case of sudden cooling (constant heat flux), is both put into perspective and extended by Equations 12, 22, and 24 of the present analysis.

Based upon the previous analysis, a conservative minimum local Rayleigh number, Ra_δ , of 3×10^3 is necessary for the onset of convection within the reservoir. According with Equation 21, the critical threshold is approximately

$$Q'' \text{Ra} > 1.8 \times 10^4 \quad (26)$$

It is now important to recognize the approximate nature of Equations 22 and 24. Both equations are related to results obtained considering a linear vertical temperature profile within the fluid (steady case). The nonlinear temperature profiles of Figure 2 suggest that, during transient cooling, a fluid layer lighter than the one for a linear temperature profile (between the same top and bottom temperatures) is developed. It is reasonable to speculate then that the actual critical Ra_δ , for time-dependent volumetric cooling, should be slightly greater than the ones used in obtaining Equations 22 and 24. (In fact, Mahler et al. (1968) estimated for a similar problem that the critical Rayleigh number might increase approximately two and a half times.)

Steady cooling results

Table 1 presents some results for a square enclosure filled with water (Pr = 7). The numerical criterion for determining onset of convection is the change (more than 0.1%) in the averaged top temperature from its conduction profile.

The underlined τ_c values refer to the most appropriate theoretical result, either from Equation 22, if τ_c (Equation 22) < τ_b , or from Equation (24), if τ_c (Equation 22) > τ_b . For $\text{Ra} = 10^4$ and $Q'' = -0.1$, the numerical simulation indicates a stable conductive cooling process. Observe that results from both Equations 22 and 24 predict critical times much larger than the time for the cooling front to reach the bottom surface

(Equation 12). Notice that $Q''Ra$, in this case equal to 10^3 , is smaller than the minimum listed in Equation 26. Also, τ_{max} (Equation 13) is smaller than τ_c from Equation 22 or 24. The $Q'' = -2$ case is also a situation where the small heat flux creates a stable layer for a long period of time, allowing the thermal front to reach the bottom of the reservoir. In this case, however, the predicted τ_b and τ_c values have the same order of magnitude, with τ_c (Equation 24) agreeing well with the numerical result.

The case $Ra = 10^6$ and $Q'' = -0.01$ is peculiar in the sense that the τ_c value from Equation 24 is supposedly the appropriate value (τ_c (Equation 22) $>$ τ_b), but in fact the numerical result agrees better with τ_c from Equation 22. This highlights the "scale basis" (approximate) nature of the theoretical predictions (in fact, in this case, the convective process is initiated before the cooling front reaches the bottom of the enclosure, so τ_b is underestimated). The general

Table 1 Critical time for onset of convection: comparison with numerical results

Ra	τ_b (eq. 12)	$-Q''$	τ_c (eq. 22)	τ_c (eq. 24)	τ_c -num.	
10^4	52.9	0.1	276.1	418.3	∞	
			2	62.0	93.5	113.0
			4	43.9	66.1	52.0
			6	35.8	54.0	37.4
			8	31.0	46.8	30.3
			18	20.6	31.2	17.1
10^6	529.1	0.01	873.1	1322.9	849.5	
			0.1	276.1	418.3	275.4
			1	87.7	132.3	82.6
			8	31.0	46.8	28.3
10^8	5291.4	0.01	873.1	1322.9	859.6	
			0.1	276.1	418.3	271.5
			2	62.0	93.5	61.4
			8	31.0	46.8	28.8

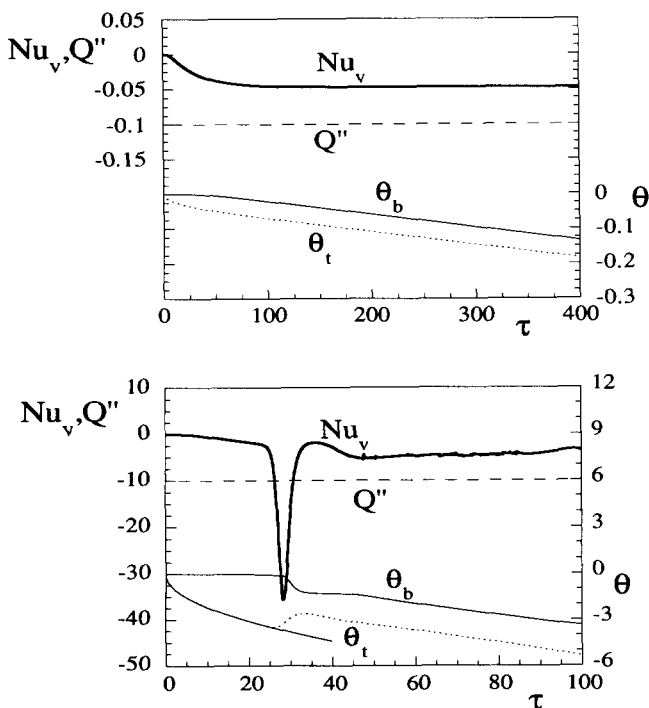


Figure 3 Constant cooling: $Ra = 10^4$. (a) $Q'' = -0.1$; (b) $Q'' = -10$

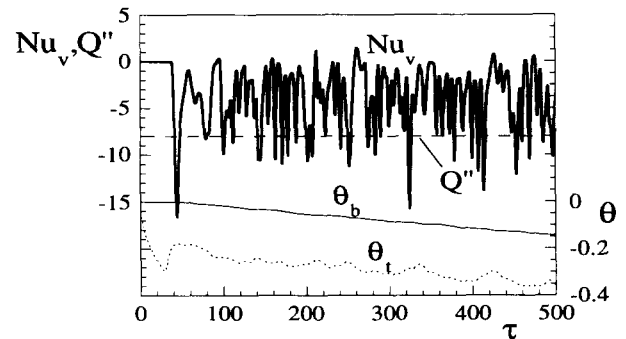
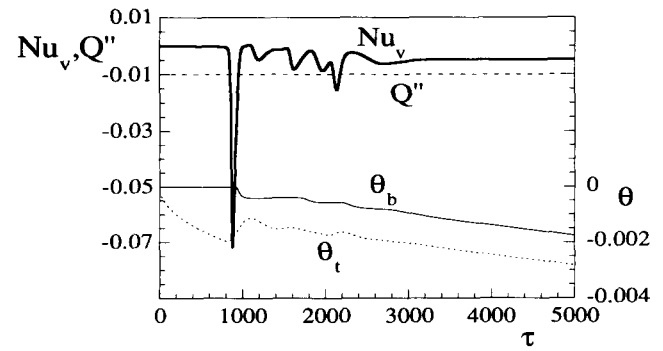


Figure 4 Constant cooling: $Ra = 10^8$. (a) $Q'' = -0.01$; (b) $Q'' = -8$

agreement between theory and numerical results is surprisingly good considering the simplifications involved.

Figure 3 shows the time evolution of the surface averaged top and bottom temperatures and the midheight averaged Nusselt number. For $Ra = 10^4$ and $Q'' = -0.1$ (Figure 3a), the cooling layer is indefinitely stable as indicated in Table 1. This observation is anticipated theoretically by recognizing that $\tau_b < \tau_c$ (Equation 22) $<$ τ_c (Equation 24). For a larger heat flux, as $Q'' = -10$ (Figure 3b), the cooling front evolves as a pure conduction layer up to the critical time, $\tau_c \sim 25.2$, when the top temperature starts to increase, indicating an upward flux of warm fluid. The initial pure conduction solution for θ_t (Equation 11) is superimposed (continuous line) on the numerical θ_t results (dashed line). The growth of disturbances after onset of convection is relatively fast as shown by the sudden drop of Nu_v and subsequent decrease in θ_b .

From the results for $Ra = 10^6$ and $Ra = 10^8$ (Table 1), it is evident that for high Rayleigh number the cooling front becomes unstable before reaching the bottom of the reservoir ($\tau_b > \tau_c$). In Figure 4a, for $Ra = 10^8$ and $Q'' = -0.01$, the system undergoes an initial conduction regime followed by a convection regime, $\tau \sim 860$, returning to a stable conductive cooling process at $\tau \sim 3000$ (observe, from Equations 7 and 11, that for steady pure conduction, $Nu_v = Q''/2$). This reflects the mixing that the first convective burst imposes in the enclosed fluid, accelerating the cooling process.

Results for $Q'' = -8$ are presented in Figure 4b. The time evolution of Nu_v indicates a very complex convective flow. One interesting feature is the almost uniform decrease in the bottom surface temperature. An enlargement of the initial convective stage is presented in Figure 5, where it is possible to verify the existence of a delay on the Nu_v response to the onset of convection. This is in agreement with the very small τ_c , when compared with τ_b , anticipated by the theoretical analysis (see Table 1), indicating a very thin cooling layer at the onset of convection.

Snapshots of the time evolution of flow and temperature fields, for the case depicted in Figure 5, are presented in Figure 6. Streamlines (left) and isotherms (right) are equally spaced, with the former defined as $\partial\Psi/\partial Y = U$ and $\partial\Psi/\partial X = -V$. The rotation of the convective cells is indicated by arrows. From top to bottom, it is noted that convection starts within regions near the corners ($\tau = 20$), with flow cells developing towards the center of the reservoir ($\tau = 30$). In each half of the domain, two cells merge and subdue a third one in between them ($\tau = 35$). At the same time, two new cells at the center and one at each side of the reservoir are developed. The continuous growth of the two center cells fuels the growth of the other cells, especially the ones near the side walls ($\tau = 40$). The thermal convective effect is to produce isotherms with an inverted mushroom-like shape in the center of the reservoir, and thermal fingers near the side walls. The fingers of cold fluid evolve in time, eventually detaching from the top layer as

droplets, explaining why the Nusselt number increases again at $\tau = 50$. These droplets migrate to the bottom of the reservoir, diffusing its thermal energy to the warm fluid. The process repeats itself in a less organized manner, resulting in the chaotic Nu_v profile observed in Figure 4.

Pulsating-heat results

The time scales given by Equations 12, 22, and 24 are used as reference for selecting heat-pulsating frequencies for the oscillatory process such that convection is induced within the reservoir. The graphs in Figures 7a to 7c show, respectively, the oscillatory behavior of the system for frequencies f equal to 0.025, 0.00625, and 0.00333, for $Ra = 10^8$ and $Q'' = -8$ ($Ra_q = -8 \times 10^8$). The corresponding half-period, Ω , is respectively equal to 20, 80, and 150.

According to Equation 23, $f = 0.025$ does not satisfy the condition for the onset of convection. However, it is seen from Figure 7a that this oscillatory mode induces convection: notice the oscillations of Nu_v and ω . This observation justifies the use of the term *sufficient condition* when the theoretical results, obtained for continuous cooling, are used for the analysis of the pulsating heat problem. When the criteria are satisfied, convection will indeed be induced. However, even when the criteria are not satisfied, the onset of convection by pulsating heat might occur due to the deformation of the fluid temperature profile within the reservoir.

Figures 7b and 7c, which show smaller frequencies satisfying the criteria for onset of convection, demonstrate the importance of ω for detecting convection. When $f = 0.00625$ (Figure 7b), the response of Nu_v is limited to the first cycle, while the peaks in ω indicate the existence of convection throughout the

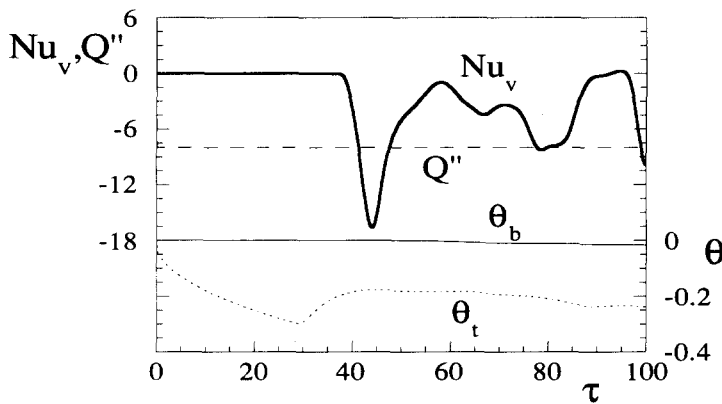


Figure 5 Constant cooling, initial stage: $Ra = 10^8$, $Q' = -8$

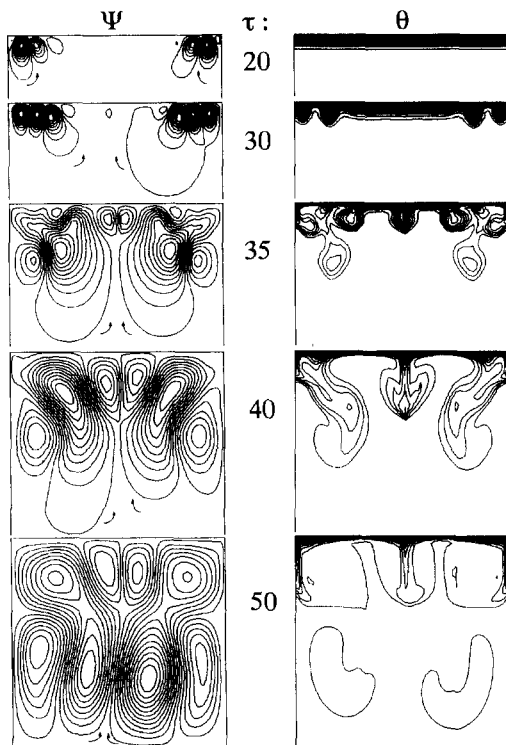


Figure 6 Time evolution of streamlines (left) and isotherms (right): $Ra = 10^8$, $Q' = -8$

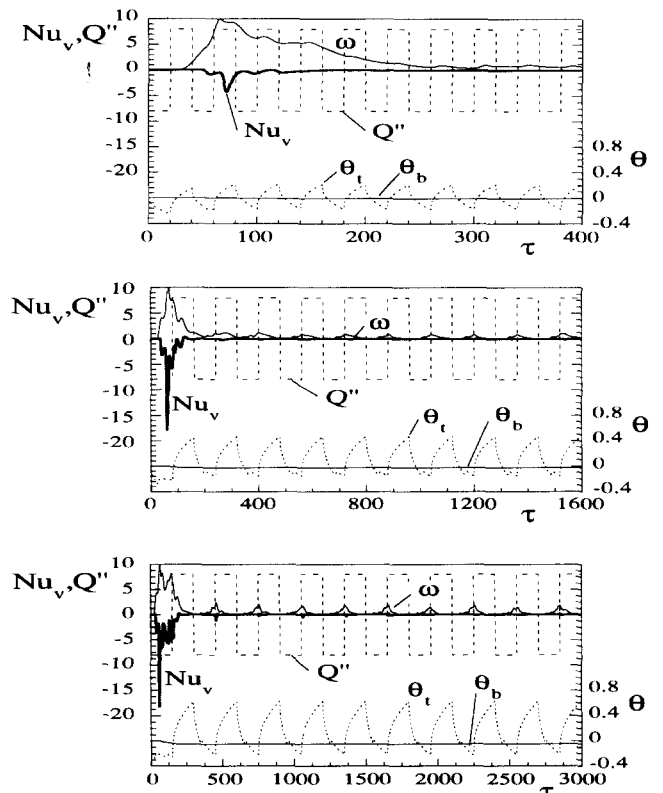


Figure 7 Pulsating heat flux, $Ra = 10^8$, $Q' = -8$. (a) $f = 0.025$; (b) $f = 0.00625$; (c) $f = 0.00333$

oscillatory process. In this case, the convective flow becomes restricted to a thin layer near the top of the reservoir, so its effect is not captured by Nu_v . Note also the asymmetry of θ , indicating the convective effect within the reservoir, namely, that of increasing the thermal resistance during the heating stage. Notice, beyond the second cycle, that the disturbances (convection) grow and decay within each cycle. This basic state is termed in the literature (Davis 1976) *transiently stable*.

In Figures 7a to 7c, the ω values are scaled so that ω_{max} is always equal to 10. The actual maximum values are, respectively, equal to 0.0184, 0.05275, 0.05127. Although it is not within the scope of the present study to ascertain the precise critical state, a suitable stability criterion that can be used for the pulsating heat case, considering the numerical constraints, is $\omega > 10^{-6}$.

Figures 8a to 8c, for $Ra = 10^8$ and $Q'' = -0.01$ ($Ra_q = -10^8$), shows results for frequency 0.0025, 0.00083, and 0.00025 (half periods of 200, 600, and 2000) respectively. In this case, the highest frequency (Figure 8a) does not induce convection, confirming the theoretical prediction (Table 1). Figure 8b, with half-period equal to 600, is in the periodic convection regime. Interestingly, the apparent frequency of convection (Nu_v and ω pulses) is approximately equal to twice the heating period. Finally, the lowest frequency (Figure 8c) promotes the strongest convective effect. Observe the waviness in the bottom temperature profile, indicating that the cooling front indeed reaches the bottom surface periodically due to the convective bursts. (In plotting Figure 8, the ω values were not scaled.)

An example of the heating/cooling process starting with heating the reservoir is illustrated in Figure 9, for $Ra = 10^8$, $Q'' = -8$, and heating period equal to 120 ($f = 0.00833$). Again, Table 1 indicates that convection should not set in. However, the pulsating effect induces convection within a thin

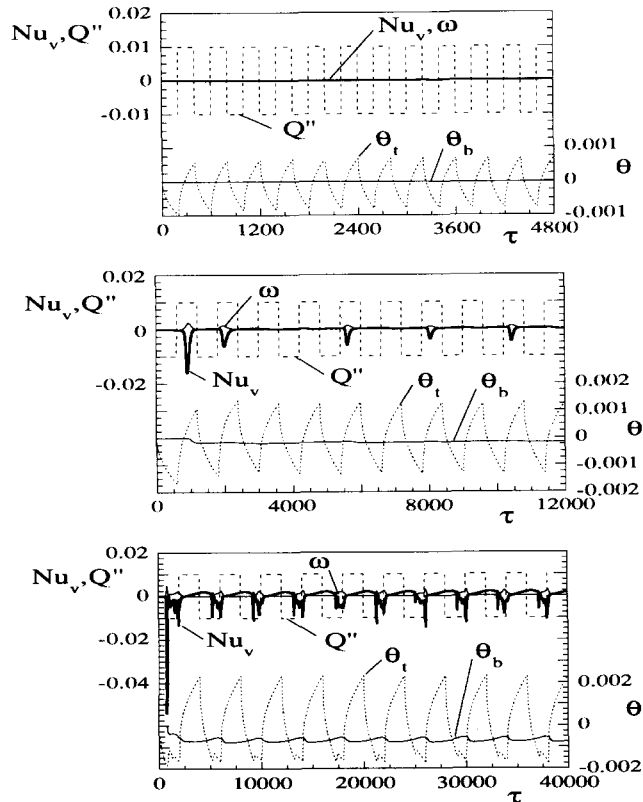


Figure 8 Pulsating heat flux, $Ra = 10^8$, $Q'' = -0.01$. (a) $f = 0.0025$; (b) $f = 0.00083$; (c) $f = 0.00025$

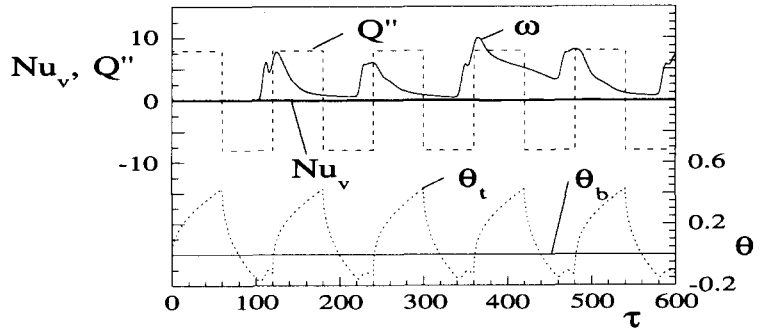


Figure 9 Pulsating heat flux (heating first), $Ra = 10^8$, $Q'' = -8$, $f = 0.0083$

layer near the top surface (notice $Nu_v = 0$). The velocity ω is scaled, having an actual maximum value equal to 0.00562.

Conclusions

A preliminary investigation of heat transfer within a fluid reservoir heated and cooled from above is performed. A theoretical analysis considering a continuously cooling transient process, based on results of similar Rayleigh-Bénard problems, is developed in order to identify an approximate condition for onset of convection. The theoretical predictions are confirmed by numerical experiments for several cases. Time evolution of streamlines and isotherms indicate the existence of very complex flow, unveiling the main characteristics of the convective process.

Using the theoretical results, the maximum frequency of heat pulsation that guarantees convective flow is obtained and tested numerically. Convection is observed for frequencies above the critical frequency, indicating that temperature gradient inversion can indeed induce convection. It is concluded then that the theoretical critical frequency is only a sufficient condition for the onset of convection by pulsating heat.

A suggestion for future research is the investigation of the critical state by linear stability analysis, considering the theoretical solution for the conduction regime as the basic state.

Acknowledgments

The author acknowledges with gratitude the support received from Southern Methodist University through the *J. L. Embrey Professorship* in Mechanical Engineering.

References

Ahlers, G., Cross, M. C., Hohenberg, P. C., and Safran, S. 1981. The amplitude equation near the convective threshold: application to time-dependent heating experiments. *J. Fluid Mech.*, **110**, 297-334
 Antohe, B. and Lage, J. L. 1994. A dynamic thermal insulator: Inducing resonance within a fluid saturated porous medium enclosure heated periodically from the side. *Int. J. Heat Mass Transfer*, **37**, 751-782
 Armfield, S. W. and Patterson, J. C. 1991. Direct simulation of wave interactions in unsteady natural convection in a cavity. *Int. J. Heat Mass Transfer*, **34**, 929-940
 Bannerot, R. B. 1992. On the determination of the averaged temperature in a horizontal storage tank and its use in monitoring the performance of a solar thermosyphon system. *J. Solar Energy Eng.*, **114**, 182-187

- Brooks, W. A. 1958. Temperature and thermal-stress distributions in some structural elements heated at a constant rate. *NACA, TN-4306*, 1-51
- Catton, I. 1972. The effect of insulating vertical walls on the onset of motion in a fluid heated from below. *Int. J. Heat Mass Transfer*, **15**, 665-672
- Chandrasekhar, S. 1961. *Hydrodynamic and Hydromagnetic Stability*. Oxford University Press, Oxford
- Davis, S. H. 1976. The stability of time-periodic flows. *Annu. Rev. Fluid Mech.*, **8**, 57-74
- Ferreira, R. F., Adams, D. B., and Davis, R. E. 1992. Development of thermal models for Hungry Horse reservoir and lake Koocanusa, northwestern Montana and British Columbia. U.S. Geological Survey, *Water-Res. Invest. Rep.*, **91-4134**, 1-30
- Foster, T. D. 1965. Stability of a homogeneous fluid layer cooled uniformly from above. *Phys. Fluids*, **8**, 1249-1257
- Frohlich, J., Laure, P., and Peyret, R. 1992. Large departures from Boussinesq approximation in the Rayleigh-Bénard problem. *Phys. Fluids A*, **4**, 1355-1372
- Imberger, J. 1985. Thermal characteristics of standing waters: an illustration of dynamic processes. *Hydrobiology*, **125**, 7-29
- Kaviany, M. 1984. Onset of thermal convection in a fluid layer subjected to transient heating from below. *J. Heat Transfer*, **106**, 817-823
- Kaviany, M. and Vogel, M. 1986. Effect of solute concentration on the onset of convection: uniform and nonuniform initial gradients. *J. Heat Transfer*, **108**, 776-782
- Kazmierczak, M. and Chinoda, Z. 1992. Buoyancy-driven flow in an enclosure with time periodic boundary conditions. *Int. J. Heat Mass Transfer*, **35**, 1507-1518
- Lage, J. L. and Bejan, A. 1993. The resonance of natural convection in an enclosure heated periodically from the side. *Int. J. Heat Mass Transfer*, **36**, 2027-2038
- Leonard, B. P. 1979. A stable and accurate convective modeling procedure based on quadratic upstream interpolation. *Comp. Meth. Appl. Mech. Eng.*, **19**, 59-98
- Lick, W. 1965. The instability of a fluid layer with time-dependent heating. *J. Fluid Mechanics*, **21**, 565-576
- Mahler, E. G., Schechter, R. S., and Wissler, E. H. 1968. Stability of a fluid layer with time-dependent density gradients. *Phys. Fluids*, **11**, 1901-1912
- Manole, D. M. and Lage, J. L. 1993. Nonuniform grid accuracy test applied to the natural convection flow within a porous medium cavity. *Numer. Heat Transfer B*, **23**, 351-368
- Mantle, J., Kazmierczak, M., and Hiawy, B. 1992. Natural convection in a horizontal enclosure with periodic changing bottom wall temperature. *National Heat Transfer Conference*, San Diego, CA. *ASME-HTD*, **198**, 49-56
- Patankar, S. V. 1980. *Numerical Heat Transfer and Fluid Flow*. Hemisphere, Washington
- Patterson, J. C. and Armfield, S. W. 1990. Transient features of natural convection in a cavity. *J. Fluid Mech.*, **219**, 469-497
- Pellew, A. and Southwell, R. V. 1940. On maintained convection motion in a fluid heated from below. *Proc. R. Soc. A*, **176**, 312-343
- Smith, E. G. 1941. The heat requirements of simple intermittently heated interior walls and furniture. *J. App. Phys.*, **12**, 642-644
- Trevisan, O. V. and Bejan, A. 1986. Convection driven by the nonuniform absorption of thermal radiation at the free surface of a stagnant pool. *Numer. Heat Transfer*, **10**, 483-506
- Vasseur, P. and Robillard, L. 1982. Natural convection in a rectangular cavity with wall temperature decreasing at a uniform rate. *Wärme- und Stoffübertr.*, **16**, 199-207
- Yang, H. Q., Yang, K. T., and Xia, Q. 1989. Periodic laminar convection in a tall vertical cavity. *Int. J. Heat Mass Transfer*, **32**, 2199-2207